LIMNOLOGY and OCEANOGRAPHY: METHODS

ASLO

Limnol. Oceanogr.: Methods 22, 2024, 805–822

doi: 10.1002/lom3.10646

Assessment of a pH optode for oceanographic moored and profiling applications

Taylor Wirth,[1]* **Yuichiro Takeshita**,[2] **Benjamin Davis**,[2] **Ellen Park**,[3] **Irene Hu**,[2] **Christine L. Huffard**,[2] **Kenneth S. Johnson**,[2] **David Nicholson**,[3] **Christoph Staudinger**,[4] **Joseph K. Warren**,[2] **Todd Martz**[1]

[1]Scripps Institution of Oceanography, University of California San Diego, La Jolla, California, USA
[2]Monterey Bay Aquarium Research Institute, Moss Landing, California, USA
[3]Woods Hole Oceanographic Institution, Woods Hole, Massachusetts, USA
[4]PyroScience GmbH, Aachen, Germany

Abstract

As global ocean monitoring programs and marine carbon dioxide removal methods expand, so does the need for scalable biogeochemical sensors. Currently, pH sensors are widely used to measure the ocean carbonate system on a variety of autonomous platforms. This paper assesses a commercially available optical pH sensor (optode) distributed by PyroScience GmbH for oceanographic applications. Results from this study show that the small, solid-state pH optode demonstrates a precision of 0.001 pH and relative accuracy of 0.01 pH using an improved calibration routine outlined in the manuscript. A consistent pressure coefficient of 0.029 pH/1000 dbar is observed across multiple pH optodes tested in this study. The response time is investigated for standard and fast-response versions over a range of temperatures and flow rates. Field deployments include direct comparison to ISFET-based pH sensor packages for both moored and profiling platforms where the pH optodes experience sensor-specific drift rates up to 0.006 pH d^{-1}. In its current state, the pH optode potentially offers a viable and scalable option for short-term field deployments and laboratory mesocosm studies, but not for long term deployments with no possibility for recalibration like on profiling floats.

The existing suite of commercially available oceanographic sensors for measuring the inorganic carbonate system is limited (Martz et al. 2015; Bushinsky et al. 2019). Commercially available pH sensors have grown in number and diversity of methodology, with current options based on electrochemical, spectrophotometric, potentiometric, and optical technology (IOCCP 2024). Glass pH electrodes have been used for decades to measure seawater pH on the benchtop. In situ glass pH electrode sensors (e.g., Idronaut, Sea-Bird Scientific SBE27, YSI EXO) are small and easily integrated into sensor packages and platforms, but suffer from reduced accuracy of ≥ 0.1 pH (Johengen et al. 2015) and sensor drift requiring frequent calibration (Martz et al. 2010; Rérolle et al. 2012).

In contrast, spectrophotometric-based instruments (e.g., Sunburst Sensors SAMI-pH, Clearwater Sensors lab on chip) have proven to be accurate to ~ 0.005 pH for long durations with low drift rates (Mowlem et al. 2021). However, their large size and long measurement intervals due to the microfluidics complexities (valves, pumps) pose challenges for fast profiling and platform integration (Yin et al. 2021).

Potentiometric pH sensors based on the Honeywell Ion Sensitive Field Effect Transistor (ISFET; Martz et al. 2010) have been successfully deployed on a wide variety of autonomous platforms and vehicles such as profiling floats (Johnson et al. 2016), underwater gliders (Saba et al. 2019; Takeshita et al. 2021*a*), moorings (Lilly et al. 2019), and autonomous surface vehicles (Chavez et al. 2018). They have been used to quantify natural variability across a wide range of marine ecosystems (Hofmann et al. 2011), estimate carbon dioxide (CO_2) fluxes (Gray et al. 2018), investigate the potential for seagrass meadows to locally ameliorate impacts of ocean acidification (Ricart et al. 2021), examine feedbacks between physical and biological forcings on seawater chemistry (Cyronak et al. 2020), quantify benthic net community production and calcification rates on coral reefs (Takeshita et al. 2018), and used as feedback control in ocean acidification mesocosm studies (Hughes et al. 2018; Donham et al. 2023). In summary, the ISFET has become a cornerstone of global ocean carbon

*Correspondence: twirth@ucsd.edu

Additional Supporting Information may be found in the online version of this article.

observing, through many observational networks worldwide such as the Integrated Ocean Observing System (IOOS, US IOOS 2021), Global Ocean Acidification Observing Network (GOA-ON, Rivest et al. 2016), and Biogeochemical Argo (Johnson et al. 2017; Claustre et al. 2020; Maurer et al. 2021).

Despite the wide breadth and usage, Honeywell, the sole producer of ISFETs widely used in DuraFET and Deep-Sea-DuraFET pH sensors, announced a halt in production in June 2022, leaving a void in the availability of scalable pH sensors for oceanographic applications. Production has since been restarted, but the potential cease in ISFET availability would have significantly hindered the ability to effectively observe the ocean carbon cycle.

Motivated to address this sole-source vulnerability in global ocean carbon observing, this study aims to contribute to the ongoing discourse on pH instrumentation by assessing a commercially available optical pH sensor, the Pico-pH-SUB pH optode, distributed by PyroScience GmbH. This optical technology, similar in design to the very popular oxygen optodes currently deployed on profiling floats and various platforms, holds promise as oxygen optode sensors have proven to be extremely robust (Tengberg et al. 2006; Bittig et al. 2018) and are indeed the most widely deployed type of chemical sensor in the ocean.

The performance of the pH optodes has been characterized in the laboratory, briefly in the field and shows promise (Fritzsche et al. 2018; Staudinger et al. 2018; Staudinger et al. 2019; Monk et al. 2021). However, further characterization focused specifically on oceanographic applications is necessary preceding widescale use of this sensor in the ocean. The objectives of this study include assessing the performance of the factory-recommended calibration procedure, developing an improved calibration method, verifying temperature response on the various calibration coefficients, quantifying response time and pressure coefficients, and assessing sensor performance and stability in different ocean environments.

This study involves deploying the pH optode on fixed platforms in the deep ocean and a highly dynamic coastal environment. Sensor drift and a proposed correction method are rigorously evaluated in these two diverse settings. In addition, the pH optode is deployed on a Spray underwater glider to assess its performance for profiling applications. Through these comprehensive analyses, a thorough assessment of the Pico-pH-SUB in multiple ocean environments is provided. The assessment generated from this study is intended to offer insights and recommendations to the broader oceanographic community. The findings contribute to advancing the understanding of pH measurement technologies, ensuring continued progress in monitoring and managing the health of marine ecosystems.

Materials and procedures

Sensor description and operating principles

We used the Pico-pH-SUB model manufactured by PyroScience GmbH (Aachen, Germany) for this study. This OEM sensor (~ 2k USD) is pressure rated to 4000 dbar and has a low power draw of 50 mW during operation (< 500 μW during sleep). Operating at a maximum sampling rate of 20 Hz, it communicates via UART protocol. The pH optode can be fully powered off in between measurements without compromising performance. For an accurate calculation of pH from the Pico-pH-SUB, a concurrent temperature measurement is required. A PT100 resistance temperature detector can be soldered directly to the Pico-pH-SUB as recommended from PyroScience GmbH, or the temperature correction can be applied post processing using an external temperature sensor, as done in this study. The performance of the Pico-pH-SUB should be identical to the other pH optodes in the PyroScience GmbH product line, such as the AquapHOx, and when integrated into a custom logger (5k–11k USD).

The pH sensitive material or "foil" is contained in the "sensor tip" which is secured by the "sensor cap" (Fig. 1a). The sensor cap also acts as a guard to protect the sensor tip. The sensor tip and cap are sold as a single assembly, separate from the optoelectronics, and installed by the user. In this study, we used both the commercially available sensor cap, and designed our own custom sensor cap to secure the sensor tip to the Pico-pH-SUB.

The pH optode's operational principle is based on the Dual Lifetime Referencing scheme (Klimant et al. 2001). The foil is comprised of an immobilized fluorescent indicator (an aza-BODIPY dye synthesized by PyroScience GmbH) and phosphorescent reference (Egyptian blue) on a support material (a PET thermoplastic). An additional outermost protective layer is equipped for optical isolation to minimize effects from direct sunlight such as oversaturation of the photodiode and bleaching of the indicator (Clarke et al. 2015; Staudinger et al. 2019). The optoelectronics utilize a 625 nm LED for excitation and a photodetector in combination with a long-pass emission filter are used to measure the luminescence intensity ratio between the pH sensitive indicator and the reference dye. The pH optode sensor signal (R) is the ratio between the indicator fluorescence intensity and reference phosphorescence intensity (Staudinger et al. 2019). This analog signal is compensated for device effects such as sensor internal temperature and signal intensity. The response of the pH optode can be described by a Boltzmann sigmoid in relation to pH (Fig. 1b and Eq. 1):

$$\mathrm{pH} = pKa' + \mathrm{slope}' \times \log\left(\frac{R1' - R2'}{R - R2'} - 1\right) + \mathrm{cal\_offset} \quad (1)$$

where $R1'$ and $R2'$ are the top and bottom asymptote terms, respectively, pKa' represents the point of inflection, $slope'$ is the slope at the point of inflection. The *cal_offset* term refers to an empirical pH offset determined during calibration and/or deployment. The prime symbol indicates the terms are at in situ temperature, and all terms expand to include the coefficient at a reference temperature of 20°C (e.g., $R1$), and a

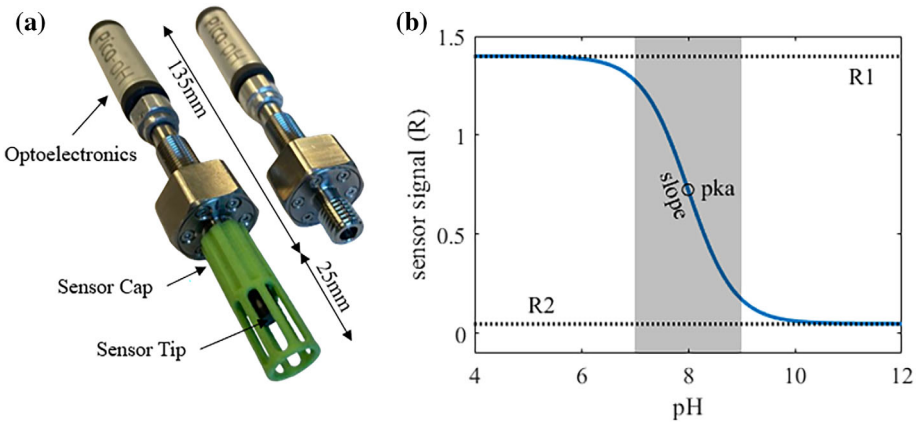

Fig. 1. (**a**) The Pico-pH-SUB sensor with and without PHCAP-PK8T-SUB sensor cap and tip installed. (**b**) Boltzmann sigmoid sensor signal R vs. pH. Nominal values of 1.4 for *R*1, 0.05 for *R*2, 8.0 for *pKa*, and 1.0 for *slope* were used. The shaded region indicates the functional pH measurement range of 7–9.

linear temperature coefficient (e.g., $R1_T$) (Eqs. 2–5). Additional salinity coefficients, pKa_{is1} and pKa_{is2}, are applied to *pKa* only:

$$R1' = R1 \times (1 + R1_T \times (T_c - 20)) \quad (2)$$

$$R2' = R2 \times (1 + R2_T \times (T_c - 20)) \quad (3)$$

$$slope' = slope \times \left(1 + slope_T \times (T_c - 20)\right) \quad (4)$$

$$pKa' = pKa + pKa_T \times (T_C - 20) - 0.5 \times pKa_{is1} \times \left[\frac{\sqrt{\frac{20\times S}{1000}}}{1+\sqrt{\frac{20\times S}{1000}}} - 0.2791745 - pKa_{is2} \times \left(\frac{20\times S}{1000} - 0.15\right)\right] \quad (5)$$

where T_C is the temperature in °C, S is practical salinity.

The PHCAP-PK8T-SUB sensor cap from PyroScience GmbH, designed to measure seawater pH on the total scale, was employed for all tests. The pH indicator material has a *pKa* of around 8, which aligns closely with the nominal ocean pH value. The sensor responds to changes in pH between 7 and 9, allowing coverage of the full range of ocean pH except in rare extreme environments. In addition, a fast-response version of this sensor tip was tested, which was custom developed for this project. The fast-response sensor tip is identical in makeup using the same pH sensitive material, but with the outermost optical protective layer removed to reduce the distance of diffusion between sample and the immobilized indicator in the foil. All laboratory tests and field deployments performed in this study were either indoors, with opaque flow manifolds or in the deep sea eliminating any negative effects due to direct sunlight.

Laboratory calibration and characterization

In the laboratory, the accuracy and assumptions associated with the manufacturer recommended calibration protocol were assessed (Three-point and temperature cycle calibration); an improved (but more time and labor intensive) calibration protocol was developed (Seawater multipoint calibration), and the pressure response (Pressure response) and the response time were quantified (Response time). Three Pico-pH-SUB units were used for sections Three-point and temperature cycle calibration and Seawater multipoint calibration. The same batch of sensor cap, thus the same batch of sensor tip and sensing material, was installed on each Pico-pH-SUB. Each sensor cap, with installed sensor tip, comes with predetermined factory coefficients from PyroScience GmbH, which are applied to the entire production batch. Three different Pico-pH-SUB units were used for section Pressure response, and two different Pico-pH-SUB units were used for section Response time. Sensor caps from the same batch were used in each section, except Pressure response, with different batches used across sections.

Three-point and temperature cycle calibration

PyroScience GmbH advises the user to conduct a 1- or 2-point calibration before initiating measurements. The first calibration point quantifies *R*1 by immersing the Pico-pH-SUB in an acidic solution of pH < 4, and the second quantifies *R*2 in a basic solution of pH > 10. An optional third point quantifies *cal_offset* using a solution with known pH. The determination of these three coefficients allows for the definition and adjustment of the sigmoid response curve, assuming the *pKa* and *slope* remain unchanged from the factory values. Among these coefficients, *R*1 and *R*2 have a nonlinear impact and can have an outsized effect on the calculated pH values (Fig. 2), underscoring the critical importance of their characterization.

For the first two calibration points, an acidic solution of pH ~ 2 was prepared using 0.08 mol L^{-1} citric acid, and a basic solution of pH ~ 11 was prepared using 0.1 mol L^{-1} sodium carbonate. Both solutions were prepared with and without a 0.7 mol L^{-1} sodium chloride (NaCl) background to compare

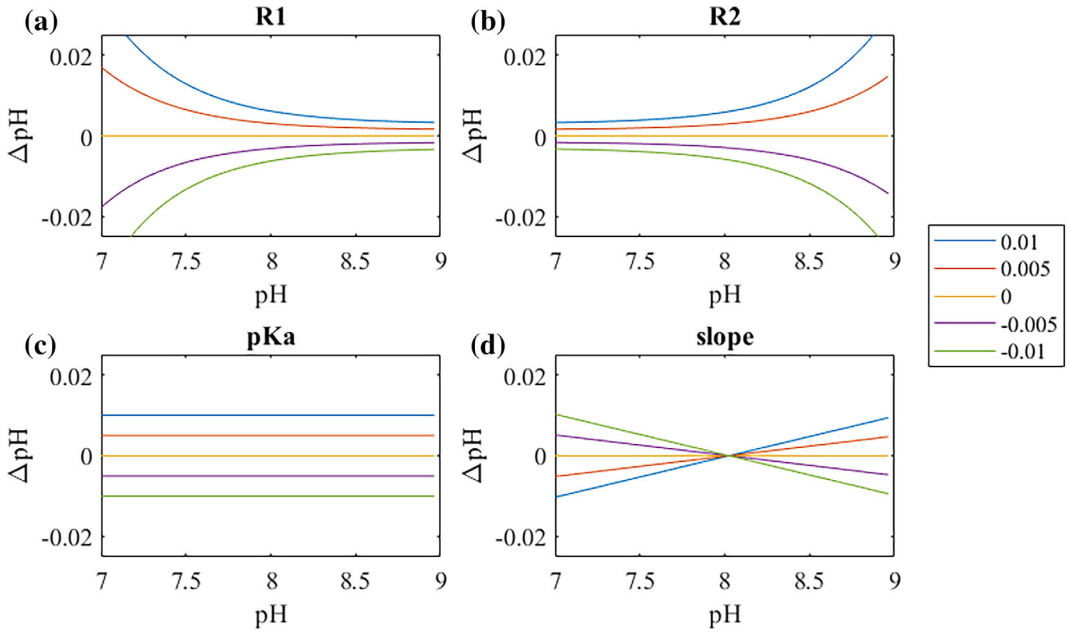

Fig. 2. The difference in calculated pH from the Pico-pH-SUB if the following sigmoid coefficient is varied by ± 0.01: (**a**) *R*1, (**b**) *R*2, (**c**) *pKa*, (**d**) *slope*. Nominal values for *R*1 = 1.5, *R*2 = 0.05, *pKa* = 8.0, *slope* = 1.0 were used.

results if a natural seawater ionic was used. PyroScience GmbH provides these solutions in small volumes to be prepared in deionized water, which posed challenges for temperature regulation and multi-day tests. Therefore, larger volume solutions were prepared for this study with separately sourced chemicals. To ensure stable readings in each solution, the Pico-pH-SUB was immersed in seawater for at least 24 h preceding the three-point calibration. Hydration of the sensing material reduced conditioning observed when a dry sensor was immersed in the acidic solution. During calibration, each solution was continuously stirred, and temperature was measured in all three solutions with a QTI DirecTemp USB thermometer (DTU6028-002), which is accurate to 0.1°C (with resolution of 0.01°C). The sensor signal, *R*, was recorded for 1 h at 1 Hz in the acidic and basic calibration solutions. *R*1 and *R*2 were calculated as the average of the final 15 readings in each solution.

The *cal_offset* was then determined by immersing the sensor in seawater with salinity of 33.5 and at 20°C, while solution pH was measured spectrophotometrically using an automated system with *meta*-cresol purple (mCP) indicator dye (Clayton and Byrne 1993; Carter et al. 2013). The biases from impurities in the mCP dye were corrected through direct comparisons with purified mCP obtained from the laboratory of R. Byrne, as described in Takeshita et al. (2021*b*). The *cal_offset* was defined as the difference between spectrophotometric pH and pH calculated from the Pico-pH-SUB, and then applied for all subsequent measurements following the calibration process.

To verify manufacturer-provided temperature coefficients ($R1_T$ and $R2_T$), the Pico-pH-SUB was operated in the acidic and basic solutions, respectively, between 5°C and 25°C, spaced at 5° intervals. Each discrete temperature step was held for a duration exceeding 2 h to allow the system and sensors to stabilize. Subsequently, the final 8 data points (spanning 2 min) for each temperature step were averaged, and a least squares linear regression was fitted. The slope of the linear regression represents the temperature coefficient.

Seawater multipoint calibration

The manufacturer recommended three-point calibration method described above assumes that the *pKa* and *slope* remain unchanged from the factory characterization. Furthermore, the *R*1 and *R*2 characterization occurs in non-seawater media, thus, matrix effects could add uncertainty to this calibration. To address these issues, we developed an automated calibration method using natural seawater that is directly traceable to spectrophotometric pH measurements, which from here on will be referred to as the "Seawater multipoint calibration." Multiple discrete spectrophotometric pH measurements were made within the functional range of the sensor (pH 7–9), and the four coefficients *R*1, *R*2, *pKa*, and *slope* were simultaneously fitted to Eqs. 1–5. This approach was conducted at a single temperature (typically 20°C) and assumed that the temperature coefficients previously determined for each sensor remain unchanged. When performed at 20°C, all the temperature dependencies in Eqs. 2–5 are minimized or zero, so no errors would propagate due to temperature coefficient uncertainty. Manufacturer values for pKa_T, $slope_T$, pKa_{is1}, and pKa_{is2} were used.

A minimum of four discrete pH points within the functional range are required to properly constrain the

multivariate optimization solver of the four sigmoid coefficients. Seawater pH was cycled between 7.4 and 8.2, at increments of 0.1 pH, resulting in nine points. This pH range was chosen to encompass the expected pH range for the field deployments in this study. Each pH increment was held for a minimum of 2 h. At the end of each pH increment, an automated spectrophotometric pH measurement was made. The seawater multipoint routine was performed three times for the three Pico-pH-SUB units to assess reproducibility and accuracy.

To conduct the seawater multipoint calibration, a customized high-precision pH and temperature control system was developed, hereafter referred to as the "pHstat system." The pHstat system utilized a 4-liter jacketed beaker connected to a recirculating temperature-controlled bath (Fisher Scientific Isotemp 4100) for maintaining temperature at specified levels. A custom cap, sealed with an O-ring, housed the sensors and tubing. The pH of the solution was controlled through a PID feedback loop that adjusted the proportion of CO_2-free gas (either pure nitrogen (N_2) or compressed air with an Ascarite II scrubber) and a 5% CO_2-air mixture that was bubbled into solution. The two gasses were mixed before delivery into the beaker, and the proportion was controlled by adjusting the flow rates of the two gasses using mass flow controllers with a range of 0–1 SLPM for the CO_2-free gas and 0–14 SCCM for the CO_2 blend (Sierra Instruments SmartTrak 50). A Honeywell DuraFET III pH sensor (51453503-501) was used as the feedback sensor for the PID control and was regularly calibrated to spectrophotometric samples. The DuraFET was chosen as it has a short-term precision of 0.0005 (Martz et al. 2010) and has a Nernstian response over a large pH range (Takeshita et al. 2014). The same spectrophotometric pH system described in section Three-point and temperature cycle calibration was integrated into the pHstat system, operating asynchronously to automatically draw samples from the jacketed beaker. The pHstat system demonstrated remarkable pH and temperature control precision, with a standard deviation of < 0.001 pH across a pH range of 7–8.5 and 0.01°C of temperature across a range of 5–30°C.

Pressure response

To determine the unknown pressure response of the Pico-pH-SUB, the sensor response was measured over a range of temperatures and pressures in a solution of known pH. For this, an equimolar tris buffer prepared in artificial seawater was utilized, as this is a standard solution for pH measurements in seawater, and its pH can be calculated over a range of temperatures and pressures (DelValls and Dickson 1998; Rodriguez et al. 2015; Takeshita et al. 2017; Müller et al. 2018). A custom pressure and temperature control (PTC) system at the Monterey Bay Aquarium Research Institute was used for this experiment. This system has been used for establishing the pressure coefficients of hundreds of Deep-Sea-DuraFET pH sensors (Johnson et al. 2016; Johnson et al. 2017).

The temperature was cycled between 5°C and 25°C at 5°C intervals. At each temperature step, pressure was cycled from 0 to 2000 dbar over an 8-h period. Temperature, pressure, and outputs from the Pico-pH-SUB were recorded at 30-s intervals. The calculated pH of tris buffer was compared against the pH output from the Pico-pH-SUB units at each temperature and pressure combination to determine the pressure response. The pressure response was characterized for three Pico-pH-SUB units, each equipped with different sensor caps for comparison across sensor material batches. Furthermore, one Pico-pH-SUB unit underwent a duplicate test to assess repeatability.

Response time

The response time for the Pico-pH-SUB was assessed for the standard-response sensor tip and a fast-response sensor tip, using two different protocols. The response time for the standard-response tip was rigorously tested in a flume with known flow velocities, whereas the response time for the fast-response tip was tested in a stirred beaker because it was not available when the flume experiments were being conducted. The results for the fast-response tip, while less quantitative regarding test controls (flow rate and temperatures), serve to demonstrate the substantial improvement in response time.

The response time of two Pico-pH-SUB units equipped with the standard-response tip was assessed within the seawater Aquatron Flume tank at Dalhousie University. Tests were performed at low and high temperatures (~ 7°C and 17°C) over a range of flow velocities from 5 to 25 cm s^{-1}, at ~ 5 cm s^{-1} increments, for both rising and falling pH step changes. The Pico-pH-SUB was first immersed in a separate temperature-controlled bath for 20 min, set to match the flume temperature. The pH of the bath was adjusted from 8.0, which was the approximate flume pH, by ~ 0.5 pH units upward or downward using sodium hydroxide or hydrochloric acid, respectively. After the 20-min conditioning period, a custom sensor cover was affixed over the Pico-pH-SUB sensor cap to trap the high or low pH solution, and the sensors were transferred to the flume. Once steady flow resumed in the flume, the sensor covers were quickly removed to produce a step change of pH. The Pico-pH-SUB measurements were recorded at 1 Hz for 20 min. Throughout all tests, the orientation of the Pico-pH-SUB remained uniform, with the sensor tip (foil surface) positioned perpendicular to the flow. This approach ensured a systematic evaluation of response times under varied conditions within the flume environment.

The response time of two Pico-pH-SUB units equipped with fast-response tips were measured by switching between two stirred seawater solutions at pH ~ 7.1 and pH ~ 8.5. Stirring speed was constant for all tests. Seawater pH was adjusted by bubbling N_2 and CO_2 gas. The temperature of both solutions was controlled at 6°C, using a 250 mL jacketed beaker. Sensors were switched between the solutions three times to assess repeatability.

Response time is reported as the time constant (63.2% or e-folding time), τ, of the exponential step response. The Pico-pH-SUB units with the standard-response sensor tips had a previous firmware version which did not utilize the *R* output but the phase shift value *dPhi* (Staudinger et al. 2018). The sensor signal (*R*) or cot(*dPhi*) measured by the Pico-pH-SUB was fit to quantify the response time. The response was initially fitted to the model:

$$y = A \times \left(1 - e^{-\frac{x}{\tau}}\right) + b \quad (6)$$

where *A* is the amplitude of the pH step change, *x* is the elapsed time starting from when the sensor cover was removed or beaker was switched, and *b* is the offset. *A* and *b* were then used to normalize the data, and the slope of the linearized Eq. 6 (outlined in Bittig et al. 2014) was used to determine the response time τ:

$$y_{\text{norm}} = 1 - e^{-\frac{x}{\tau}} \quad (7)$$

Field deployments

The in situ performance of the pH optode was assessed through three field deployments: a nearly yearlong deployment at 4000 m depth off the coast of California, a 2.5-month deployment in a shallow, dynamic coastal environment in Southern California, and on a Spray underwater glider that profiled to 1000 m off the Central California Coast.

Station M

Two AquapHOx-LX were deployed at 4000 m depth on a benthic lander at Station M (34.5°N, 123°W; Smith et al. 1983) off the coast of California for approximately 1 yr (09 October 2021–29 September 2022). One unit was secured just above the seafloor or benthic boundary layer (labeled as "BBL"), and the other 1 m above the seafloor (labeled as "1m"; Fig. 3a). The AquapHOx-LX is a data logger distributed by PyroScience GmbH that houses the Pico-pH-SUB using the standard-response sensor tip and an integrated thermistor. Measurement interval was set to 10 min. The Pico-pH-SUB units were calibrated using the three-point method before deployment. These Pico-pH-SUB units also had a previous firmware version which reported *dPhi* instead of *R*, but performance is comparable between versions as hardware characteristics of the sensor did not change between versions. Even though these units do not provide a direct comparison with the current firmware versions used throughout this study, the year-long deployment provides insights into long-term drift in a deep, cold, and stable environment. The measured pH was compared against pH estimated using an empirical algorithm (ESPER-LIR, Carter et al. 2021). ESPER-LIR inputs included temperature measured by the AquapHOx-LX, estimated oxygen of 133 μmol/kg and salinity (PSS-78) of 34.68 (Smith et al. 2022), and estimated nitrate of 37 μmol kg^{-1} derived from GLODAP V2.2022 (Lauvset et al. 2022), location and date. The uncertainty of the ESPER-LIR input oxygen is 1%, consistent with the historic variability at Station M from weekly oxygen measurements between 2015 and 2020 using a benthic rover (Supporting Information Fig. S1a; Smith et al. 2021). The remaining ESPER input uncertainties were set to 0.003 for temperature and salinity and 2% for nitrate.

Scripps pier

The Pico-pH-SUB was deployed alongside a Self-Calibrating SeapHOx (SCS) at Scripps Pier in La Jolla, CA for ~ 2.5 months (18 July–05 October 2023). The SCS is a sensor package containing a DuraFET pH sensor and is capable of autonomous in situ calibration with tris buffer prepared in artificial seawater (Bresnahan et al. 2021). Deployment depth was approximately 4 m, fixed to a pier piling. The nearshore environment experiences seasonal wind-driven upwelling, where pH and temperature can be as low as ~ 7.7 and 10.5°C, respectively, even at shallow depths (Kekuewa et al. 2022). The Pico-pH-SUB was integrated into its own housing with a custom controller to poll and record the measurements at 10-min intervals. A custom sensor cap was developed to house the standard-response sensor tip, which included an O-ring seal and separate flow manifold (Fig. 3b). The outflow of the SCS was directly plumbed to the flow manifold of the Pico-pH-SUB, which ensured a pumped flow stream to the sensor tip and allowed for a direct comparison of the measurements. In addition, two automated tris buffer injections of the SCS flowed through the Pico-pH-SUB manifold to provide high quality validation samples.

Prior to deployment, the Pico-pH-SUB was calibrated using (1) the three-point calibration with factory temperature coefficients, (2) the three-point calibration with sensor-specific re-determined temperature coefficients, and (3) the multipoint calibration with re-determined temperature coefficients. Calibration methods 1 and 2 were highly similar, resulting in exclusion of method 2 from the discussion below. The pH reported by the SCS was calibrated to the automated tris buffer injections performed during the deployment, following the methodology outlined in Bresnahan et al. (2021). Two discrete bottle samples were collected, poisoned, and analyzed on a spectrophotometric system using purified mCP.

Using the two automated tris buffer injections, an in situ adjustment to *cal_offset* and drift correction method is explored. To determine the optimal number of validation samples required, an analysis involving the hypothetical collection of 2–10 validation samples uniformly spaced between the deployment's start and end dates was conducted.

Spray glider

The Pico-pH-SUB was integrated onto a Spray underwater glider (Sherman et al. 2001) to evaluate the sensor performance on profiling platforms. The Spray glider was also equipped with a Deep-Sea-DuraFET (DSD) pH sensor (Johnson et al. 2016; Takeshita et al. 2021*a*), allowing for a direct comparison between the two pH sensors. A custom housing with a

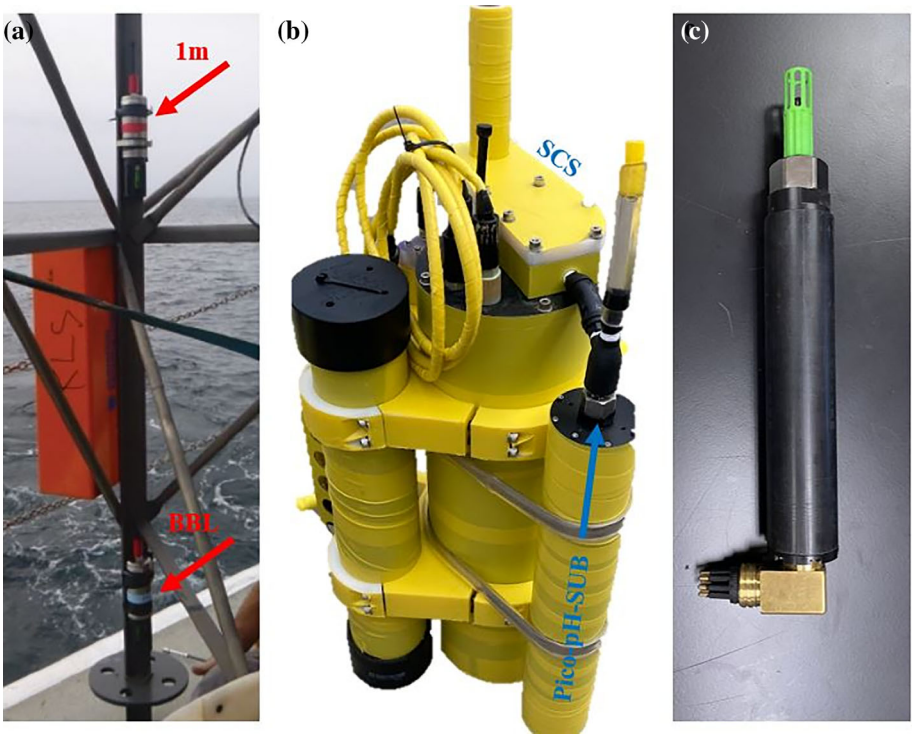

Fig. 3. (**a**) Two Pico-pH-SUB loggers (AquapHOx-LX, red arrows) mounted on a benthic lander. (**b**) The Self-Calibrating SeapHOx (SCS) pictured with the Pico-pH-SUB (blue arrow) housing. (**c**) The Pico-pH-SUB housing with SubConn connector used to integrate into the Spray glider. Flow manifold not shown.

flow manifold designed to fit around the factory sensor cap was fabricated for the Pico-pH-SUB and integrated into the pumped flow stream of the Spray glider (Fig. 3c). The Pico-pH-SUB was powered and polled by the main glider controller and measured on both the ascent and descent for some profiles to assess performance between the two, which would indicate errors due to slow sensor response. The Pico-pH-SUB underwent the pre-deployment temperature cycle and seawater multipoint calibration procedures.

Two missions were conducted to ~ 25 km offshore in Monterey Bay, CA, with maximum dives to 1000 m. The first mission (15 February–02 March 2023) utilized the standard-response sensor tip, whereas the second mission (10–17 July 2023) utilized the fast-response sensor tip. For both missions, dives were conducted to 500 m, then dive depths were sequentially increased to 1000 m at 100-m intervals, while making measurements on both the ascent and descent. Unfortunately, the cabling to the DSD failed during the first mission, thus, the Pico-pH-SUB with the standard foil was compared to pH estimated from CANYON-B (Bittig et al. 2018), as this algorithm estimates pH accurately near Monterey Bay, particularly at depths below 300 m (Takeshita et al. 2021*a*). The Pico-pH-SUB with the fast-response sensor tip was directly compared to the DSD for the second mission. For each mission, the difference between algorithm pH and pH measured by the Pico-pH-SUB for the first dive below 900 dbar determined the *cal_offset* applied to every profile. The pressure coefficient determined in this study was also applied to every profile. The DSD data were adjusted following Takeshita et al. (2021*a*).

Assessment

Three-point and temperature cycle calibration

The addition of 0.7 mol L^{-1} NaCl in the acidic solution produced an increase in *R*1 of 0.0433 ± 0.0008 for the three Pico-pH-SUB units. This offset in *R*1 changes calculated pH depending on the solution pH. For example, pH can shift by ~ 0.03 at pH 8, and ~ 0.05 at pH 7.6 due to a 0.05 shift in *R*1. As *R*1 is the acidic asymptote, there is a larger effect at lower pH values (Fig. 2). This was a surprising, yet repeatable effect that was not reported in previous studies (Staudinger et al. 2018) and highlights the importance of characterizing *R*1 in a solution with similar ionic strength as the target environment. On the other hand, there was no shift in *R*2 observed with the NaCl addition, indicating that it can be characterized without the addition of NaCl, which simplifies solution preparation.

Values for the *R*1, *R*2, and *cal_offset* coefficients obtained using the three calibration methods for the three Pico-pH-SUB units are shown in Table 1. Large variability in *R*1 was observed between the three units and had a range of ~ 0.08

Table 1. Coefficients for three Pico-pH-SUB units, determined by varying calibration methods. *R*1 and *R*2 for the temperature cycle method were determined by interpolating a linear regression to 20°C.

		Three-point			Temperature cycle			Seawater multipoint		
	Pyro Sci	Pico 1	Pico 2	Pico 3	Pico 1	Pico 2	Pico 3	Pico 1	Pico 2	Pico 3
R1	1.6181	1.5920	1.5633	1.5115	1.4201	1.4004	1.3551	1.4900	1.4692	1.4141
R2	0.0579	0.0399	0.0309	0.0285	0.0278	0.0120	0.0168	0.0039	0.0040	0.0045
pKa	8.0840	-	-	-	-	-	-	8.1174	8.1109	8.1101
slope	1.0340	-	-	-	-	-	-	1.0226	1.0150	1.0126
$R1_T$	−0.0008	-	-	-	−0.0031	−0.0031	−0.0030	-	-	-
$R2_T$	−0.0011	-	-	-	0.0016	0.0016	0.0016	-	-	-
cal_offset	-	0.0509	0.0475	0.0434	-	-	-	-	-	-
Date	-	11 Oct 2023			31 Oct 2023			08 Dec 2023		

during each calibration. The relative magnitude of *R*1 between the sensors were consistent across each calibration (e.g., Pico 1 had the highest *R*1 during each calibration), indicating that the differences in observed *R*1 reflect real differences in the calibration coefficient. Furthermore, all *R*1 values obtained in this study were significantly lower than the manufacturer assigned value. These results suggest that each sensor tip should be calibrated individually for *R*1 to obtain the most accurate results. On the other hand, the variability between sensors for the other three coefficients were smaller, with a range of ~ 0.01 for *R*2, 0.007 for *pKa*, and 0.01 for *slope*. This indicates that batch calibration may be sufficient for these coefficients. While these values were slightly different from the manufacturer assigned values, the resulting biases are < 0.01 pH (Fig. 2), unless measuring solution pH of > 8.5, where biases may increase to > 0.01. Therefore, it may be sufficient to utilize the manufacturer provided values for *R*2, *pKa*, and *slope* for most applications where accuracy of pH better than 0.01 are not required, requiring only a single point calibration in acidic solution. However, to achieve the highest accuracy possible, it is recommended to individually calibrate each Pico-pH-SUB with its respective sensor tip for all three coefficients.

Accurate temperature coefficients must be established if the Pico-pH-SUB is to be used over a wide range of temperatures. There was excellent agreement in the $R1_T$ and $R2_T$ between each Pico-pH-SUB unit (Table 1; Supporting Information Fig. S2), suggesting that the temperature coefficients are consistent across the same sensor tip batch. However, there was a small difference of ~ 0.0025 between the temperature coefficients provided by the manufacturer and those determined by this study ($R1_T$ was lower, and $R2_T$ was higher relative to the manufacturer values). A difference of this magnitude for $R1_T$ results in a maximum difference of calculated pH of 0.03 at 5°C or 35°C (vs. 20°C), while at pH 8 (Supporting Information Fig. S3). The larger the deviation from 20°C, the greater the difference in calculated pH.

The $R2_T$ coefficient determined by the temperature cycle method was opposite in sign than compared to the factory-determined value (Table 1). The change in $R2_T$ does not affect calculated pH as significantly as $R1_T$ for most oceanographic applications, since its impact is larger as solution pH increases above ~ 8.1 (*pKa*). A difference of 0.0025 for $R2_T$ equates to a maximum pH difference of only ~ 0.002 at 5°C or 35°C (Supporting Information Fig. S3). A lower pH yields a lower pH difference for this change in $R2_T$, ~ 0.001 at pH 7.6. The presence of NaCl did not alter the slope, hence the temperature coefficients are not affected by a salinity background.

Seawater multipoint calibration

Results from the seawater multipoint calibrations for three Pico-pH-SUB units indicate that the measurements were within ± 0.004 pH for a single calibration run against spectrophotometric measurements between pH 7.4–8.2 (Fig. 4a). This is derived from the range of all residuals between the pH optodes and the spectrophotometric measurements. These residuals are comparable with those from the DuraFET. The calibration can be further improved if the pH range is reduced. Reducing the range to 7.8–8.1 pH produced residuals of ± 0.002 between the Pico-pH-SUB and spectrophotometric samples. However, errors for measurements outside of the pH fit range increase substantially and can be as high as 0.1, highlighting the tradeoff associated with choice of calibration range. For each pH step of the seawater multipoint method, the precision (standard deviation) of the calculated pH output of the Pico-pH-SUB after calibration was ± 0.0006. For comparison, the DuraFET pH precision was ± 0.0004 demonstrating that the pHstat system was reliably stable and precise at each pH step.

The short-term accuracy of ± 0.004 pH was only achievable during single calibration runs. To investigate the repeatability of the seawater multipoint calibration method over multiple runs, coefficients determined from the first run were applied to three subsequent runs for a single Pico-pH-SUB unit,

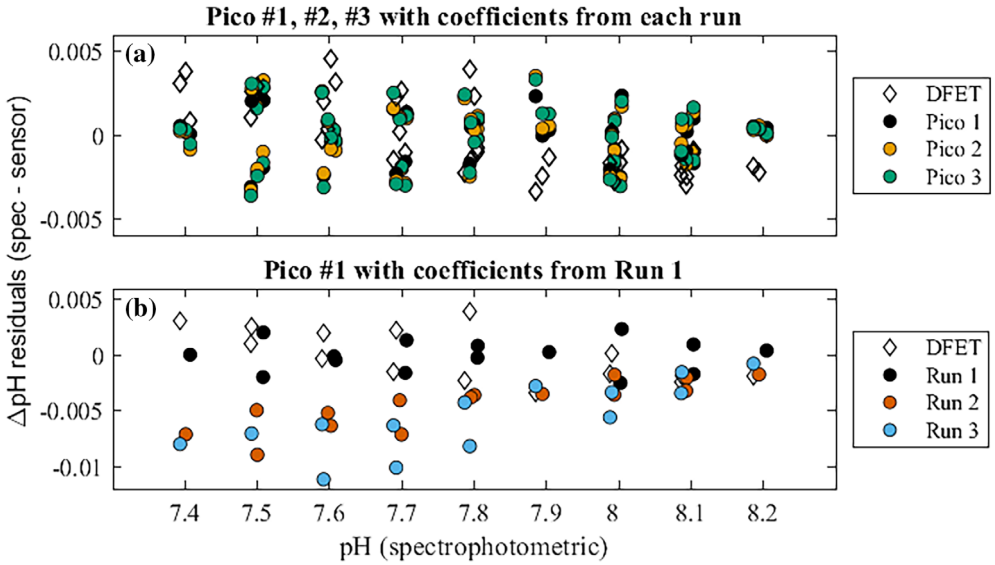

Fig. 4. (**a**) Residuals between spectrophotometric pH and the DuraFET pH (open diamonds) and pH calculated from the Pico-pH-SUB (filled circles) for three Pico-pH-SUB units during a seawater multipoint calibration. (**b**) Residuals between spectrophotometric pH and the DuraFET pH (open diamonds) and a single Pico-pH-SUB unit using coefficients from run 1 applied to sequential seawater multipoint calibration runs (filled circles).

conducted over 1 week (Fig. 4b). The residuals around the *pKa*, pH ∼ 8, remained consistent between the calibration runs, but the magnitude of the residuals increased to ∼ 0.01 pH at lower solution pH. Results were equivalent for all three Pico-pH-SUB units. Thus, we report a relative accuracy for the Pico-pH-SUB to be 0.01 over the nominal ocean pH range of 7.4–8.2.

If the PyroScience factory coefficients or three-point calibration coefficients were used to calculate pH during the seawater multipoint routine, residuals to the spectrophotometric samples were between 0.1 and 0.3 across the calibration range. This was anticipated, as the coefficients were established months before the seawater multipoint calibration. We conclude that drift, particularly in the *R*1 coefficient, invalidated the factory calibration. This emphasizes the importance of calibrating the Pico-pH-SUB as close as possible to time of use.

Pressure dependence

During the temperature and pressure cycling, the pH of the tris buffer was calculated as a function of temperature and pressure and compared to the pH output of the Pico-pH-SUB units. During pressurization, the pH of the tris buffer decreased while pH output from the Pico-pH-SUB increased (Fig. 5a). There was no pressure input for internal data processing on the Pico-pH-SUB, so the increase in pH observed in the Pico-pH-SUB output represents all combined pressure effects on the foil including the chemical properties of the fluorescent indicator.

When comparing the Pico-pH-SUB pH output to known pH of the tris buffer across the pressure range, there was good agreement across the three units and the replicates of Pico-pH-SUB unit 4 were almost identical to each other (Fig. 5b). Negligible effect in the pressure response was seen due to temperature. Thus, a constant pressure response of 0.029 pH/1000 dbar is recommended for all Pico-pH-SUB units. It is unknown if this response remains valid above 2000 dbar but was assumed applicable to the full 4000 dbar rating due to the linear relationship seen in this study. Further testing is required to verify the pressure coefficient above 2000 dbar.

Response time

The response time ranged from 195 to 750 s for the standard-response sensor tip, depending on temperature, and whether pH was increasing or decreasing (Fig. 6). In general, the direction of pH change played a significant role in response time, with a rising pH producing longer τ compared to falling pH at all temperatures. Average τ for both Pico-pH-SUB units at lower temperatures (∼ 7°C) were 298 ± 34 s for falling and 660 ± 76 s for rising pH changes. Higher temperatures (∼ 17°C) produced an average τ of 245 ± 48 s for falling and 378 ± 64 s for rising pH changes. Flow rate had a negligible impact on response time, which suggests that either diffusion within the sensor tip is the dominant process controlling the response time, or that the flow rates tested here with the sensor foil faced perpendicular to the flow was insufficient to significantly alter the boundary layer thickness at the sensor-water interface (Frankær and Sørensen 2019).

The τ values from this study were larger than reported in a previous study which stated response times of 125 s at 25°C and 145 s at 4°C for a similar pH sensitive material (Staudinger et al. 2019). They did not explore bidirectional changes in pH, or effects from flow rates. It is not clear why there was such a difference between the two studies.

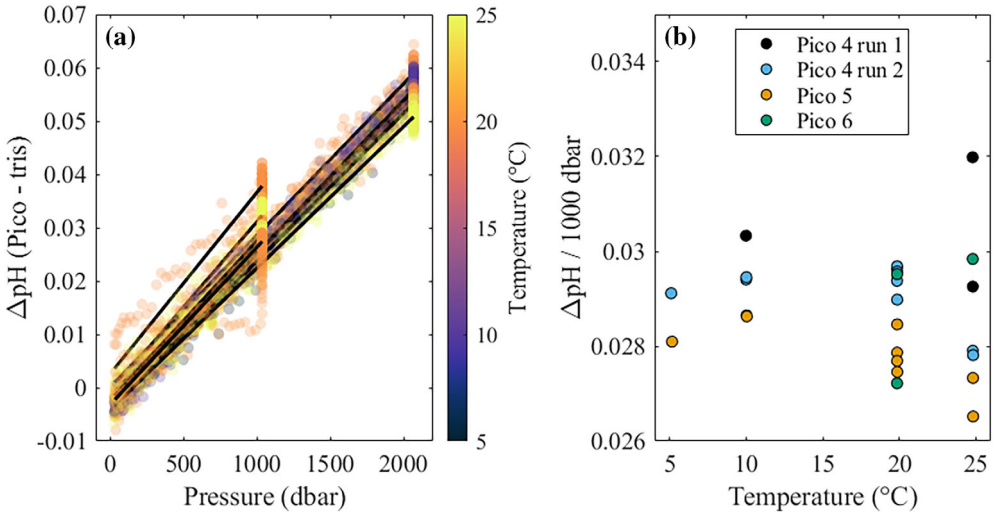

Fig. 5. (**a**) Difference in pH between the Pico-pH-SUB and tris buffer over 2000 dbar colored by temperature. Points correspond to both increasing and decreasing pressure. The black lines are the linear regression for each pressurization cycle at stable temperatures. (**b**) The difference in pH per 1000 dbar (slope magnitudes in (**a**)) for each Pico-pH-SUB. Pico 4 was temperature and pressure cycled twice.

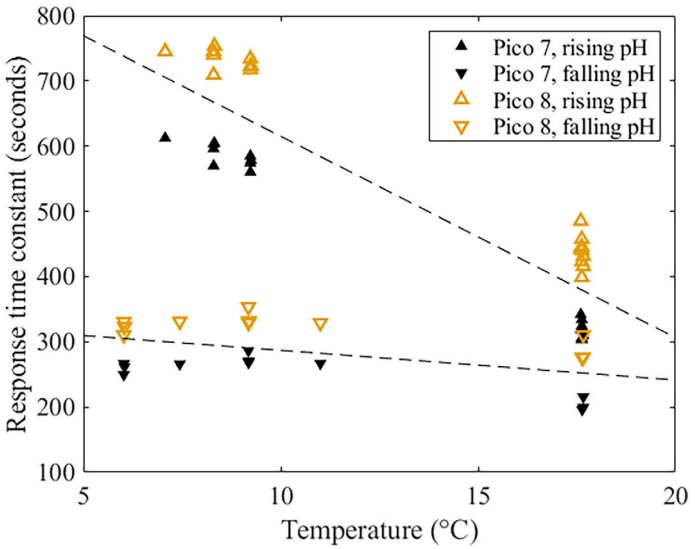

Fig. 6. Response time for two Pico-pH-SUB units with standard-response sensor tips as a function of temperature. Upward triangles represent a rising pH step change. Downward triangles represent a falling pH step change. Dashed lines are linear regressions through the rising and falling points, applied to both Pico-pH-SUB units.

The response time for the fast-response sensor tip was approximately 10 times faster than the standard foil (Table 2): 19 ± 3 s for falling and 62 ± 19 s for rising pH changes. These values align with the only previous study using the fast-response sensor tip (Staudinger et al. 2018). We did not explore the temperature effects on the response time of the fast-response sensor tip, but response time would decrease with increasing temperature, if diffusion processes control response time as hypothesized.

Table 2. Average response time constants (63.2%) for the Pico-pH-SUB from this study and previous literature. The downward arrow (↓) corresponds to tests done with falling pH step changes, upward arrow (↑) corresponds to rising pH step changes. The asterisk (*) represents the response time reported in each respective study, not necessarily the response time constant. The dash (-) represents unknown or not mentioned values.

Reference	Sensor tip type	Temperature (°C)	τ_{63} (s)
This study	Standard	7	298↓–659↑
		17	245↓–378↑
This study	Fast	6	19↓–62↑
Staudinger et al. (2019)	Standard	4	145↑
		25	125↑
Fritzsche et al. (2018)	-	-	20*
Staudinger et al. (2018)	Fast	-	< 60*

Field deployments

Station M

Throughout the nearly yearlong deployment, the temperature recorded by the AquapHOx-LX sensors remained stable, exhibiting a mean of 1.360 ± 0.006°C. Although there was a difference of ~0.12°C from the temperature reported by Smith et al. (2021) (Supporting Information Fig. S1b), the focus of this study lies more on the stability of the deep conditions and pH measurements than on absolute accuracy.

An initial conditioning of the Pico-pH-SUB loggers, lasting approximately 3 weeks was observed, yet the cause, whether pressure or temperature-related remains uncertain (Fig. 7). An

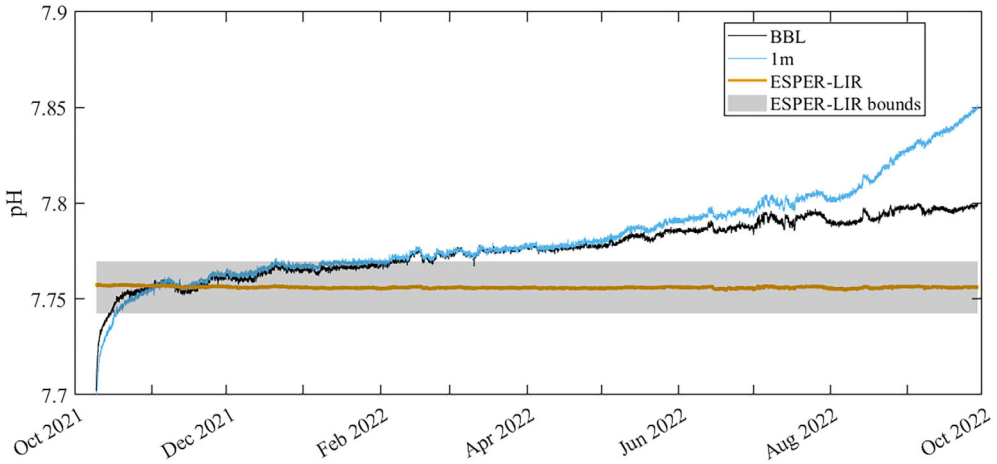

Fig. 7. Time series of two Pico-pH-SUB loggers attached to a bottom lander approximately 4000 m deep at Station M. One logger was just above the benthic boundary layer (BBL, black line) and another 1 m above the bottom (1m, blue line). A linearly interpolated regression (ESPER-LIR, yellow line) was estimated for the time series, with uncertainty bounds shown (shaded region). The logger pH values were adjusted to ESPER-LIR 21 d after deployment on 01 November 2021.

additional in situ *cal_offset* was applied at the 21-d mark on 01 November 2021 (0.063 pH for BBL logger and 0.016 pH for 1m logger) to facilitate visualization of sensor performance compared to the stable ESPER-LIR pH estimate.

Both sensors exhibited significant drift in the cold and stable environment, surpassing ESPER-LIR estimated uncertainty bounds of $\pm$ 0.014 within 3 months. Drift rates of the two sensors were nearly consistent for the first 6 months at a rate of 0.00016 pH d^{-1}. After 6 months the BBL logger continued a near linear drift while the 1m sensor drift increased significantly up to a maximum of 0.0008 pH d^{-1}.

Scripps pier

The nearshore environment at Scripps Pier exhibited a temperature range of 13–24°C and a pH range of 7.9–8.3 during the deployment (Fig. 8; Supporting Information Fig. S4). The SCS underwent two automated tris injections for sensor validation and correction, which yielded mean residuals within $\pm$ 0.004 pH between the SCS and in situ tris buffer pH values. The tris corrected SCS pH residuals to the two discrete bottle samples showed a consistent offset of -0.034 ± 0.016 pH, indicating no significant drift for the SCS pH. We are aware of this offset between the tris buffer and bottle sample residuals but maintain the methodology outlined in Bresnahan et al. (2021) to calibrate to the fourfold more consistent tris buffer injections. The deployment was divided into two periods: (1) 18 July–15 August 2023, characterized by stable conditions, and (2) 15 August–05 October 2023, marked by increased pH variability and significant drift of the Pico-pH-SUB.

During the first period, the mean difference between the Pico-pH-SUB and SCS was 0.108 ± 0.010 for the three-point calibration method and 0.004 ± 0.012 for the seawater multipoint method (Fig. 8). In the subsequent period of the deployment, the Pico-pH-SUB exhibited an increasing linear drift compared to the SCS for both calibration methods.

The availability of automated tris injections presented an opportunity for in situ adjustment of *cal_offset* and drift correction. The process involved calculating the difference between the in situ pH of the tris buffer at the time of injection and the pH recorded by the Pico-pH-SUB (Fig. 9). The adjusted *cal_offset* was then applied from the beginning of the deployment (18 July) to the first tris injection (15 August). A linear regression was fit from the first tris injection (15 August) to the second tris injection (12 September). This regression slope was then applied to the remaining measurements of the deployment after the first tris injection. The correction results were similar if the discrete bottle samples were used instead of the tris injections. Applying this correction to both calibration methods did not alter the results for the first month of the deployment besides improving the offset of the three-point calibration method to be more aligned with the SCS.

The in situ adjusted *cal_offset* applied to the multipoint calibration method at the first tris injection was negligible, measuring less than 0.001 pH. In contrast, the in situ adjusted *cal_offset* applied to the three-point calibration method was 0.082 pH. This in situ *cal_offset* adjustment relative to the first tris buffer injection is less than the difference between the Pico-pH-SUB and the SCS described above (0.108). This discrepancy may be due to the three-point calibration method deviating in accuracy away from the *pKa* of the sensor as the in situ pH of the tris buffer was $\sim$ 8.3 for the first injection, or from a slower response to rising pH changes.

During the second period of the deployment, drift rates determined by the linear regression between the first and second tris injections were consistent for both calibration methods, measuring at 0.002 pH d^{-1}, aligning with previous

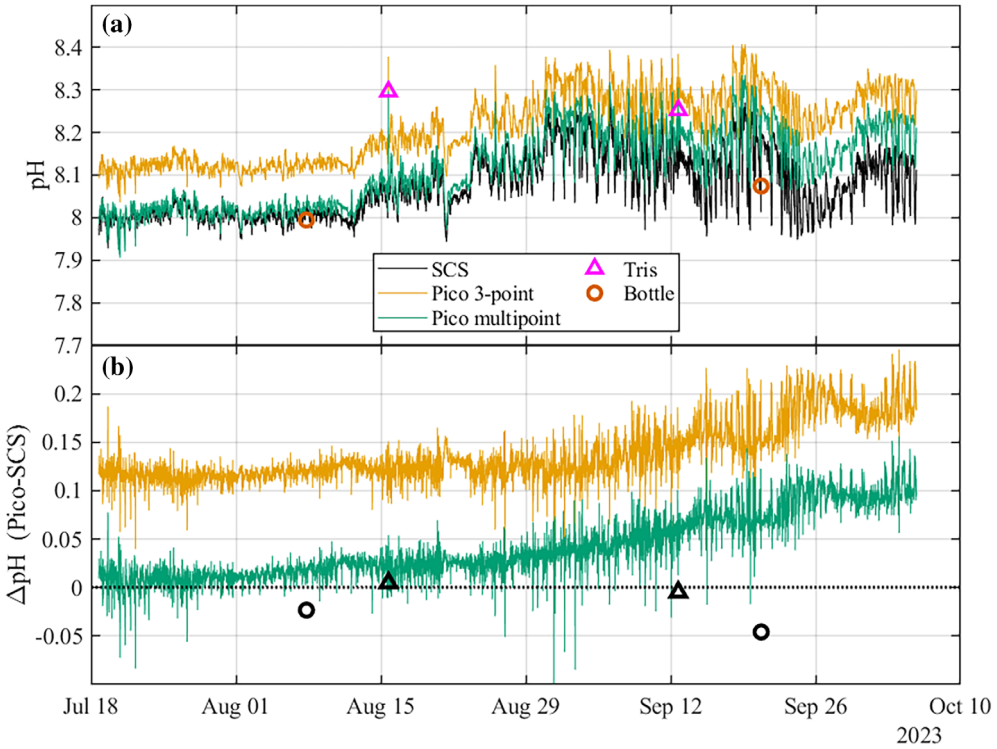

Fig. 8. (**a**) Time-series from Scripps Pier of tris-corrected Self-Calibrating SeapHOx (SCS) pH (black line) and uncorrected pH from the Pico-pH-SUB calculated using the pre-deployment three-point calibration (yellow line) and seawater multipoint calibration (green line). Discrete tris buffer (magenta triangles) and bottle samples (orange circles) also shown. (**b**) Difference between the Pico-pH-SUB and SCS pH for both calibration methods (yellow and green lines) and the difference between discrete samples (tris and bottle) in situ pH and SCS pH (black triangles and circles, respectively).

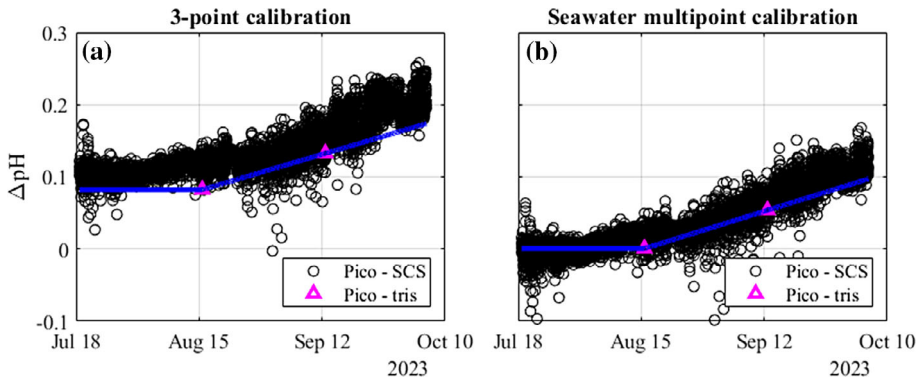

Fig. 9. (**a**) Difference in pH between the Pico-pH-SUB and Self-Calibrating SeapHOx (SCS) for the three-point calibration. (**b**) Difference in pH between the Pico-pH-SUB and SCS for the seawater multipoint calibration method (right). In situ pH offset and linear correction shown in blue lines corrected to the tris injections (magenta triangles).

studies (Fritzsche et al. 2018; Staudinger et al. 2018; Staudinger et al. 2019).

Post deployment in situ adjustments of *cal_offset* resulted in significantly improved agreement over the entire deployment (Fig. 10a). For the duration of the deployment, after the corrections to tris buffer were applied, residuals between the Pico-pH-SUB with the three-point calibration and the SCS were 0.027 ± 0.015, while those with the multipoint calibration were 0.010 ± 0.014. Both calibration methods exhibited good alignment with the SCS, although a larger difference was still observed for the three-point calibration method as previously noted. An observable reduction in the amplitude of Pico-pH-SUB measurements was observed in the second half of the deployment during coincident low pH and temperature

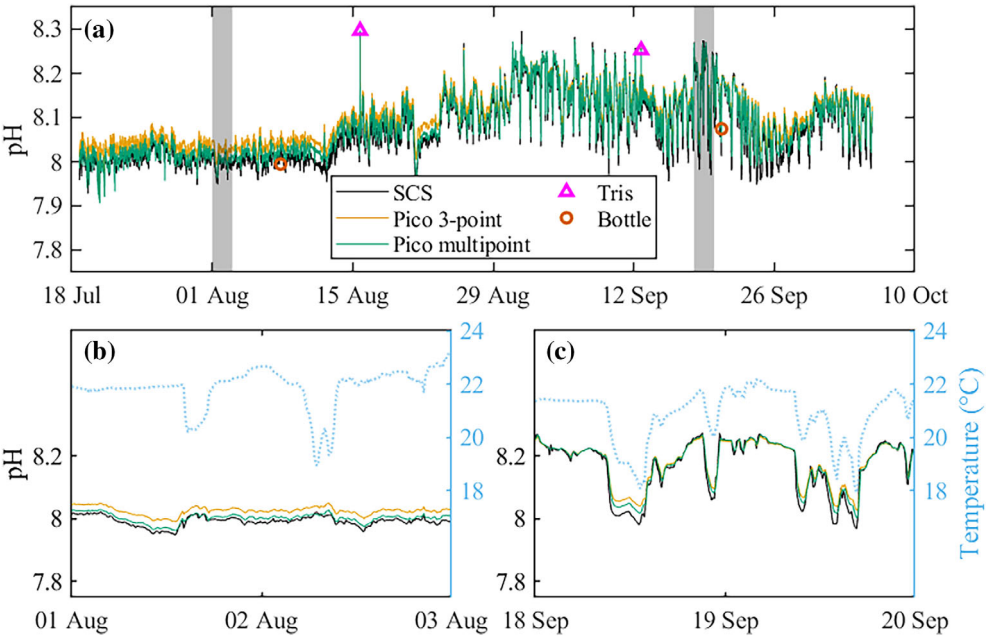

Fig. 10. (**a**) Time-series of the Self-Calibrating SeapHOx (SCS, black line) and Pico-pH-SUB with *cal_offset* adjustment and linear drift correction applied to both the three-point calibration method (yellow line) and seawater multipoint calibration (green line). Shaded regions show a zoom in between 01–03 August (**b**) and 18–20 September 2023 (**c**) with temperature (blue dashed line).

excursions (Fig. 10c). While some of the reduced amplitude of the Pico-pH-SUB relative to the SCS might be attributable to sensor lag, the sustained period of several hours on 18 September where the Pico-pH-SUB never "catches up" to the SCS may indicate a pH-dependent calibration error that is not captured by adjustments to *cal_offset* alone.

To assess the number of corrections necessary to recover data from a drifting Pico-pH-SUB, 2–10 simulated validation points were performed relative to the SCS (Supporting Information Fig. S5; $n = 6$ shown). This exercise indicated that an increase in the number of validation samples beyond two did not contribute to the improvement of Pico-pH-SUB correction, where the mean and standard deviation of the Pico-pH-SUB corrected pH relative to the hypothetical validation samples remained unchanged. This finding suggests that only two validation samples taken every 4 weeks was sufficient to correct the drift for this deployment.

Spray glider

The Pico-pH-SUB functioned properly throughout both glider missions, demonstrating the capability to withstand repeated profiles to 1000 dbar. Over multiple dives, Pico-pH-SUB measurements at depths below 800 dbar (where pH is generally constant) agreed to better than 0.003, which is comparable to the performance of the DSD (Johnson et al. 2016; Takeshita et al. 2021*a*,*b*). However, the standard-response sensor tip experienced a large hysteresis that reached > 0.1 pH near the surface between ascending and descending profiles (Fig. 11a). An additional *cal_offset* of 0.05 pH was required to align the Pico-pH-SUB with CANYON-B estimates below 900 dbar. Relative to the estimated pH from the CANYON-B algorithm, the Pico-pH-SUB pH was lower on the descent and higher on the ascent in the upper part of the water column. This pattern indicates that this hysteresis was caused by the slow response time of the sensor. In theory, the slow response time can be accounted for, as is done for oxygen optodes (Bittig et al. 2018). However, applying corrections with a response time of 400 s using this approach resulted in excessively noisy readings > 0.5 pH throughout the entire profile.

In contrast, the fast-response sensor tip exhibited significantly smaller hysteresis between ascending and descending profiles (Fig. 11b). The magnitude of the hysteresis was < 0.02 pH. Small scale vertical variability and features were captured by the Pico-pH-SUB above 300 dbar, similar to the DSD. However, there was a large discrepancy between the DSD and Pico-pH-SUB utilizing pre-deployment calibration coefficients for this deployment. These Pico-pH-SUB profiles appeared skewed and muted, indicating a sigmoid shift between pre-deployment calibration and deployment. The cause of this shift remains unknown, but potential sources include the expulsion of an air bubble between the sensor tip and optoelectronics during pressurization or movement of the screw-on sensor tip.

Immediately following the fast-response sensor tip recovery, the Pico-pH-SUB underwent a post-deployment recalibration using the seawater multipoint method. Applying these post-deployment calibrations resulted in improved alignment with the DSD pH, demonstrating that the calibration coefficients did in fact shift before deployment. This is

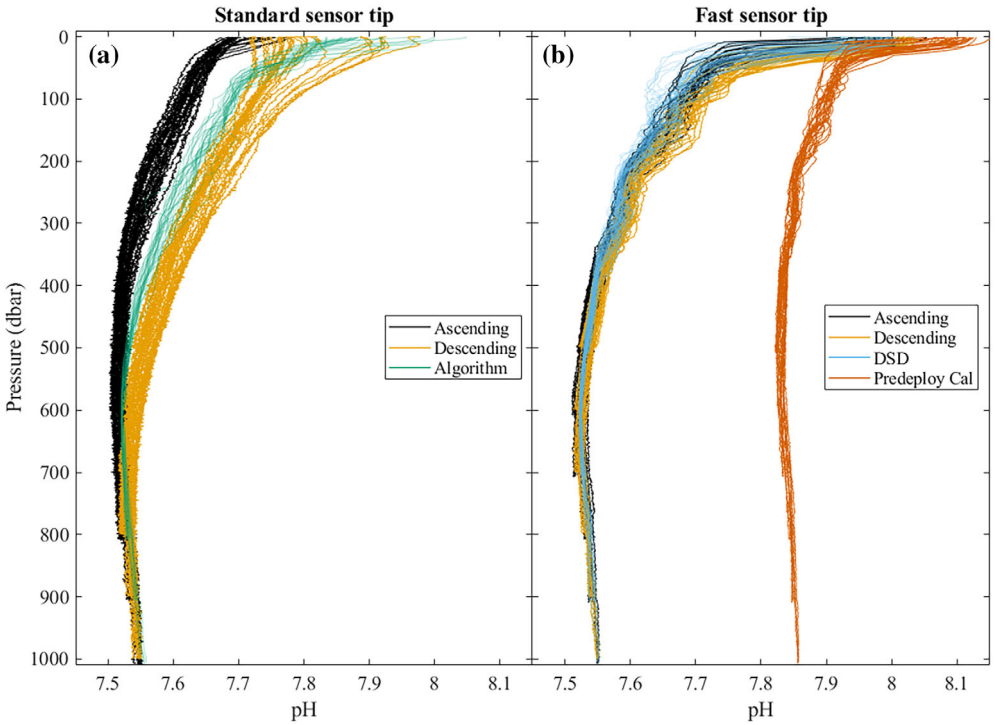

Fig. 11. (**a**) Profiles of the standard-response sensor tip that measured on both the ascent (black) and descent (yellow), greater than 500 dbar. CANYON-B algorithm (green) calculated for ascending profiles only. (**b**) Ascending and descending profiles of the fast-response sensor tip down to 500 dbar and deeper utilizing post-deployment calibration coefficients (black and yellow). Profiles using pre-deployment calibration coefficients are shown for ascending profiles only (orange). Ascending Deep-Sea DuraFET (DSD) profiles (blue) were only available on the fast-response sensor tip deployment.

troubling, as the pH optode was calibrated within 1 week of deployment on the glider. An additional *cal_offset* of 0.081 pH was required to align the Pico-pH-SUB with CANYON-B estimates below 900 dbar. Ascending profiles exhibited improved alignment with DSD profiles, likely influenced by increasing temperature and shortened response time during ascent.

During the short deployments, Pico-pH-SUB profiles displayed drift discernable for both the standard and fast-response sensor tips (Supporting Information Fig. S6). To calculate the drift rate, ascending profiles starting from depths over 500 dbar were selected. The mean pH value between 500 and 600 dbar was calculated for only ascending profiles to exclude hysteresis effects, and because this range had more profiles where pH was assumed to be stable. A linear regression of mean pH with time yielded drift rates of 0.005 pH d^{-1} for the standard-response sensor tip and 0.006 pH d^{-1} for the fast-response sensor tip at an average temperature of $\sim 6°C$. No drift was observed for the DSD.

Discussion

In this study, we conducted a thorough assessment of the Pico-pH-SUB pH optode for oceanographic applications, aiming to evaluate its potential as an alternative pH sensor to currently available technologies. Multiple calibration methods were scrutinized, with the seawater multipoint method yielding the most accurate results as it determines all four sigmoid coefficients within the functional range in natural seawater media. This calibration method had a relative, short-term accuracy of 0.004 in the lab over a pH range of 7.4–8.2 compared against spectrophotometric measurements. The accuracy was improved when analyzed over a smaller pH range, ~ 0.002 for pH 7.8–8.1. This accuracy would only apply to measurements immediately following calibration, and only over this range. Repetitions over 1 week resulted in an accuracy of 0.01 for the full range (7.4–8.2), which is applicable to most practices using the Pico-pH-SUB and the accuracy reported here. The residuals were largest at lower pH values, suggesting that the $R1$ coefficient was potentially drifting or changing between calibration runs, or a pH-dependent drift was present. The offset in $R1$ during the three-point calibration due to NaCl addition highlights the importance of using solutions with similar ionic strength or composition as the target solution. Calibration should be carried out as close in time to deployment as possible, and an additional *cal_offset* may be required once the sensor is deployed.

Minor variances were noted in $R1_T$ and $R2_T$ when comparing manufacturer-provided values with those derived from the temperature cycle method. The changes in calculated pH due to changes in $R1_T$ and $R2_T$ are small, but for applications

spanning large temperature and pH ranges they can be significant. These variances were attributed to methodological disparities between this study and those from the manufacturer. PyroScience temperature coefficients were determined by subjecting artificial seawater to temperature cycling across the functional pH range. Producing the temperature coefficients at the top and bottom of the asymptote will provide a more robust and repeatable value, but determining the coefficients in seawater may be advantageous for oceanographic applications, analogous to the seawater multipoint methodology.

Drift was observed across all field deployments, ranging from 0.0002 pH d^{-1} (deep, cold environment), 0.002 pH d^{-1} (shallow, dynamic environment) to 0.006 pH d^{-1} (profiling). The unexplained initial conditioning of approximately 3 weeks only observed during the Station M deployment raises concerns for short-term deployments in the deep sea. It is implied that Pico-pH-SUB units with sensor tips from the same batch may exhibit similar drift for the initial 6 months but may be batch-dependent. The difference in drift rates seen throughout the study suggests that they were temperature and pH dependent. Lower temperature deployments had lower drift rates, and lower in situ pH had higher drift rates. The presence of nonlinear drift rates complicates drift correction, emphasizing the need for further exploration and quantification of these phenomena.

Despite a relatively long response time of the standard-response sensor tip, the pH optode effectively tracked dynamic pH variability in the near-shore environment at Scripps Pier, showcasing comparable performance to the SCS and DuraFET pH sensor. The multipoint calibration method proved to be a more accurate calibration approach, but both calibration methods captured the dynamic variability nearly equally once an in situ *cal_offset* adjustment was applied. This in situ *cal_offset* adjustment is similarly used for oxygen optodes that experience calibration shifts between the lab and field (Takeshita et al. 2013; Bittig et al. 2018). The larger in situ *cal_offset* adjusted value of 0.082 pH for the three-point calibration method is due to the seawater multipoint method's characterization of sigmoid over the desired the pH range and its timing, performed 2 months before the seawater multipoint method.

Using the automated in situ tris buffer validation samples proved to be a robust method for correcting the initial offset and linear drift. By examining a range of hypothetical validation samples, taking more than two samples did not improve the correction, suggesting that taking validation samples every 4 weeks is sufficient. However, caution is advised against delaying validation sample collection too long after the start of deployment, as sensor drift may have already influenced the data, potentially leading to an overestimation of the in situ *cal_offset* adjustment.

The standard-response sensor tip proved unsuitable for profiling applications. The fast-response sensor tip showed promise for profiling applications but experienced a calibration shift between the lab and deployment. For long-term profiling applications, like profiling floats, which are typically not recovered, post-deployment calibration of the sigmoid coefficients is challenging. Extrapolating the drift rate observed for the fast-response sensor tip, the expected drift rate would be 0.06 pH per profile for a standard 10-d profiling interval for BGC-Argo floats, which would be unacceptably large.

In its current state, the Pico-pH-SUB seems best suited for short-term deployments on the order of weeks to months, aimed to capture weather-scale pH variability of 0.02 (Newton et al. 2015). With careful attention to calibration, the sensor could provide high-quality short-term measurements on shipboard rosette profiles and underway mapping applications in addition to shore-based experiments such as controlling or monitoring pH levels for mesocosm studies focused on ocean acidification and marine carbon dioxide removal experiments (Bockmon et al. 2013; Fuhr et al. 2024). The swappable sensor tips, uncomplicated three-point calibration and sensor integration make it a valuable addition to the short list of viable pH sensor technologies available to the oceanographic community.

Comments and recommendations

From this work, here we outline recommendations for Pico-pH-SUB users to achieve the highest quality data possible:

- Hydrate the sensor tip in sea water for at least 24 h preceding any measurements.
- Temperature cycling to verify $R1_T$ and $R2_T$ is simple, and the coefficients can be applied to an entire batch of sensor tips. This is most likely unnecessary for most applications, as these coefficients do not greatly affect calculated pH.
- For laboratory calibration, the seawater multipoint method is the most accurate, but likely too difficult and time intensive for most users.
  - The three-point calibration proved to be comparable in performance and is recommended for most users. Only two-points may be sufficient (*R*1 and *R*2) as *cal_offset* adjustment will most likely be required after the laboratory calibration.
  - Performing either calibration method as close to time of deployment may minimize the *cal_offset* adjustment.
  - Laboratory calibration should be performed in solutions similar in ionic strength to the deployment location.
- An in situ *cal_offset* adjustment based on a discrete validation sample taken alongside the sensor may be required and is recommended to be conducted early in the deployment (< 1 week) before drift takes over.
- It may be possible to correct for drift with multiple validation samples taken throughout the deployment. Validation samples every 3–4 weeks and at the end of the deployment are recommended to maintain the weather objective quality of 0.02 pH.
- Short-term profiling applications on Spray gliders or other profiling platforms would require use of the fast-response

sensor foil, with sensor refinement to reduce or eliminate the potential for offsets between calibration and deployment. Recoverable, short-term deployments may allow for post-deployment re-calibration.

References

Bittig, H. C., B. Fiedler, R. Scholz, G. Krahmann, and A. Körtzinger. 2014. Time response of oxygen optodes on profiling platforms and its dependence on flow speed and temperature. Limnol. Oceanogr.: Methods **12**: 617–636. doi:10.4319/lom.2014.12.617

Bittig, H. C., and others. 2018. Oxygen optode sensors: Principle, characterization, calibration, and application in the ocean. Front. Mar. Sci. **4**: 429. doi:10.3389/fmars.2017.00429

Bockmon, E. E., C. A. Frieder, M. O. Navarro, L. A. White-Kershek, and A. G. Dickson. 2013. Technical note: Controlled experimental aquarium system for multi-stressor investigation of carbonate chemistry, oxygen saturation, and temperature. Biogeosciences **10**: 5967–5975. doi:10.5194/BG-10-5967-2013

Bresnahan, P. J., and others. 2021. Autonomous in situ calibration of ion-sensitive field effect transistor pH sensors. Limnol. Oceanogr.: Methods. **19**: 132–144. doi:10.1002/lom3.10410

Bushinsky, S. M., Y. Takeshita, and N. L. Williams. 2019. Observing changes in ocean carbonate chemistry: Our autonomous future. Curr. Clim. Change Rep. **5**: 207–220. doi:10.1007/s40641-019-00129-8

Carter, B. R., J. A. Radich, H. L. Doyle, and A. G. Dickson. 2013. An automated system for spectrophotometric seawater pH measurements. Limnol. Oceanogr.: Methods **11**: 16–27. doi:10.4319/lom.2013.11.16

Carter, B. R., and others. 2021. New and updated global empirical seawater property estimation routines. Limnol. Oceanogr.: Methods **19**: 785–809. doi:10.1002/lom3.10461

Chavez, F. P., J. Sevadjian, C. Wahl, J. Friederich, and G. E. Friederich. 2018. Measurements of pCO_2 and pH from an autonomous surface vehicle in a coastal upwelling system. Deep-Sea Res. II: Top. Stud. Oceanogr. **151**: 137–146. doi:10.1016/j.dsr2.2017.01.001

Clarke, J. S., E. P. Achterberg, V. M. C. Rérolle, S. Abi Kaed Bey, C. F. A. Floquet, and M. C. Mowlem. 2015. Characterisation and deployment of an immobilised pH sensor spot towards surface ocean pH measurements. Anal. Chim. Acta **897**: 69–80. doi:10.1016/j.aca.2015.09.026

Claustre, H., K. S. Johnson, and Y. Takeshita. 2020. Observing the global ocean with biogeochemical-Argo. Annu. Rev. Mar. Sci. **12**: 23–48. doi:10.1146/annurev-marine-010419-010956

Clayton, T. D., and R. H. Byrne. 1993. Spectrophotometric seawater pH measurements: Total hydrogen ion concentration scale calibration of *m*-cresol purple and at-sea results. Deep-Sea Res. I: Oceanogr. Res. Pap. **40**: 2115–2129. doi:10.1016/0967-0637(93)90048-8

Cyronak, T., and others. 2020. Diel temperature and pH variability scale with depth across diverse coral reef habitats. Limnol. Oceanogr.: Lett. **5**: 193–203. doi:10.1002/lol2.10129

DelValls, T. A., and A. G. Dickson. 1998. The pH of buffers based on 2-amino-2-hydroxymethyl-1,3-propanediol ('tris') in synthetic sea water. Deep-Sea Res. Part 1 Oceanogr. Res. Pap. **45**: 1541–1554. doi:10.1016/S0967-0637(98)00019-3

Donham, E. M., I. Flores, A. Hooper, E. O'Brien, K. Vylet, Y. Takeshita, J. Freiwald, and K. J. Kroeker. 2023. Population-specific vulnerability to ocean change in a multistressor environment. Sci. Adv. **9**: eade2365. doi:10.1126/sciadv.ade2365

Frankær, C. G., and T. J. Sørensen. 2019. Investigating the time response of an optical pH sensor based on a polysiloxane–polyethylene glycol composite material impregnated with a pH-responsive triangulenium dye. ACS Omega **4**: 8381–8389. doi:10.1021/acsomega.9b00795

Fritzsche, E., and others. 2018. A validation and comparison study of new, compact, versatile optodes for oxygen, pH and carbon dioxide in marine environments. Mar. Chem. **207**: 63–76. doi:10.1016/j.marchem.2018.10.009

Fuhr, M., and others. 2024. Alkaline mineral addition to anoxic to hypoxic Baltic Sea sediments as a potentially efficient CO_2-removal technique. Front. Clim. **6**: 1338556. doi:10.3389/fclim.2024.1338556

Gray, A. R., and others. 2018. Autonomous biogeochemical floats detect significant carbon dioxide outgassing in the high-latitude Southern Ocean. Geophys. Res. Lett. **45**: 9049–9057. doi:10.1029/2018GL078013

Hofmann, G. E., and others. 2011. High-frequency dynamics of ocean pH: A multi-ecosystem comparison. PLoS One **6**: e28983. doi:10.1371/journal.pone.0028983

Hughes, B. B., S. C. Lummis, S. C. Anderson, and K. J. Kroeker. 2018. Unexpected resilience of a seagrass system exposed to global stressors. Glob. Change Biol. **24**: 224–234. doi:10.1111/gcb.13854

International Ocean Carbon Coordination Project (IOCCP). 2024. Instruments and sensors: Hardware pH directory. Accessed 7 August 2024. https://www.ioccp.org/index.php/hardware-listing/hardware-ph

Johengen, T., G. J. Smith, D. Schar, M. Atkinson, H. Purcell, D. Loewensteiner, Z. Epperson, and M. Tamburri. 2015. Performance Demonstration for Autonomous pH sensor technologies, UMCES Technical Report Series: Ref. No. [UMCES] CBL 2015-008, CBL 2015-009, CBL 2015-010, CBL 2015-011, CBL 2015-012, CBL 2015-013, CBL 2015-014. Accessed 7 August 2024. http://www.act-us.info/

Johnson, K. S., H. W. Jannasch, L. J. Coletti, V. A. Elrod, T. R. Martz, Y. Takeshita, R. J. Carlson, and J. G. Connery. 2016. Deep-Sea DuraFET: A pressure tolerant pH sensor designed for global sensor networks. Anal. Chem. **88**: 3249–3256. doi:10.1021/acs.analchem.5b04653

Johnson, K. S., and others. 2017. Biogeochemical sensor performance in the SOCCOM profiling float array. J. Geophys. Res.: Oceans **122**: 6416–6436. doi:10.1002/2017JC012838

Kekuewa, S. A. H., T. A. Courtney, T. Cyronak, and A. J. Andersson. 2022. Seasonal nearshore ocean acidification and deoxygenation in the Southern California Bight. Sci. Rep. **12**: 17969. doi:10.1038/s41598-022-21831-y

Klimant, I., C. Huber, G. Liebsch, G. Neurauter, A. Stangelmayer, and O. S. Wolfbeis. 2001. Dual lifetime referencing (DLR)—A new scheme for converting fluorescence intensity into a frequency-domain or time-domain information, p. 257–274. *In* B. Valeur and J. C. Brochon [eds.], New trends in fluorescence spectroscopy. Springer. doi:10.1007/978-3-642-56853-4_13

Lauvset, S. K., and others. 2022. GLODAPv2.2022: The latest version of the global interior ocean biogeochemical data product. Earth Syst. Sci. Data **14**: 5543–5572. doi:10.5194/essd-14-5543-2022

Lilly, L. E., U. Send, M. Lankhorst, T. R. Martz, R. A. Feely, A. J. Sutton, and M. D. Ohman. 2019. Biogeochemical anomalies at two Southern California Current System moorings during the 2014–2016 warm anomaly-El Niño sequence. J. Geophys. Res.: Oceans **124**: 6886–6903. doi:10.1029/2019JC015255

Martz, T. R., J. G. Connery, and K. S. Johnson. 2010. Testing the Honeywell Durafet® for seawater pH applications. Limnol. Oceanogr.: Methods **8**: 172–184. doi:10.4319/lom.2010.8.172

Martz, T., K. Daly, R. Byrne, J. Stillman, and D. Turk. 2015. Technology for Ocean Acidification Research: Needs and availability. Oceanography **25**: 40–47. doi:10.5670/oceanog.2015.30

Maurer, T. L., J. N. Plant, and K. S. Johnson. 2021. Delayed-mode quality control of oxygen, nitrate, and pH data on SOCCOM biogeochemical profiling floats. Front. Mar. Science **8**: 683207. doi:10.3389/fmars.2021.683207

Monk, S. A., and others. 2021. Detecting and mapping a CO_2 plume with novel autonomous pH sensors on an underwater vehicle. Int. J. Greenhouse Gas Control **112**: 103477. doi:10.1016/j.ijggc.2021.103477

Mowlem, M., and others. 2021. Industry partnership: Lab on chip chemical sensor technology for ocean observing. Front. Mar. Sci. **8**: 697611. doi:10.3389/fmars.2021.697611

Müller, J. D., F. Bastkowski, B. Sander, S. Seitz, D. R. Turner, A. G. Dickson, and G. Rehder. 2018. Metrology for pH measurements in brackish waters—Part 1: Extending electrochemical pHT measurements of Tris buffers to salinities 5–20. Front. Mar. Sci. **5**: 176. doi:10.3389/fmars.2018.00176

Newton, J. A., R. A. Feely, E. B. Jewett, P. Williamson, and J. Mathis. 2015. Global ocean acidification observing network: Requirements and governance plan. GOA-ON Global Ocean Acidification Observing Network. https://www.iaea.org/sites/default/files/18/06/goa-on-second-edition-2015.pdf

Rérolle, V. M. C., C. F. A. Floquet, M. C. Mowlem, D. P. Connelly, E. P. Achterberg, and R. R. G. J. Bellerby. 2012. Seawater-pH measurements for ocean-acidification observations. TrAC Trends Anal. Chem. **40**: 146–157. doi:10.1016/j.trac.2012.07.016

Ricart, A. M., and others. 2021. Coast-wide evidence of low pH amelioration by seagrass ecosystems. Glob. Change Biol. **27**: 2580–2591. doi:10.1111/GCB.15594

Rivest, E. B., M. O'Brien, L. Kapsenberg, C. C. Gotschalk, C. A. Blanchette, U. Hoshijima, and G. E. Hofmann. 2016. Beyond the benchtop and the benthos: Dataset management planning and design for time series of ocean carbonate chemistry associated with Durafet®-based pH sensors. Eco. Inform. **36**: 209–220. doi:10.1016/j.ecoinf.2016.08.005

Rodriguez, C., F. Huang, and F. J. Millero. 2015. The partial molal volume and compressibility of Tris and Tris–HCl in water and 0.725 m NaCl as a function of temperature. Deep-Sea Res. I: Oceanogr. Res. Pap. **104**: 41–51. doi:10.1016/j.dsr.2015.06.008

Saba, G. K., and others. 2019. The development and validation of a profiling glider deep ISFET-based pH sensor for high resolution observations of coastal and ocean acidification. Front. Mar. Sci. **6**: 664. doi:10.3389/FMARS.2019.00664

Sherman, J., R. E. Davis, W. B. Owens, and J. Valdes. 2001. The autonomous underwater glider "spray". IEEE J. Oceanic Eng. **26**: 437–446. doi:10.1109/48.972076

Smith, K. L., Jr., M. B. Laver, and N. O. Brown. 1983. Sediment community oxygen consumption and nutrient exchange in the central and eastern North Pacific. Limnol. Oceanogr. **28**: 882–898. doi:10.4319/lo.1983.28.5.0882

Smith, K. L., Jr., A. D. Sherman, P. R. McGill, R. G. Henthorn, J. Ferreira, T. P. Connolly, and C. L. Huffard. 2021. Abyssal Benthic Rover, an autonomous vehicle for long-term monitoring of deep-ocean processes. Science Robotics **6**: eabl4925. doi:10.1126/scirobotics.abl4925

Smith, K. L., Jr., M. Messié, T. P. Connolly, and C. L. Huffard. 2022. Decadal time-series depletion of dissolved oxygen at abyssal depths in the Northeast Pacific. Geophys. Res. Lett. **49**: e2022GL101018. doi:10.1029/2022GL101018

Staudinger, C., and others. 2018. A versatile optode system for oxygen, carbon dioxide, and pH measurements in seawater with integrated battery and logger. Limnol. Oceanogr.: Methods **16**: 459–473. doi:10.1002/lom3.10260

Staudinger, C., M. Strobl, J. Breininger, I. Klimant, and S. M. Borisov. 2019. Fast and stable optical pH sensor materials for oceanographic applications. Sens. Actuators B Chem. **282**: 204–217. doi:10.1016/j.snb.2018.11.048

Takeshita, Y., T. R. Martz, K. S. Johnson, J. N. Plant, D. Gilbert, S. C. Riser, C. Neill, and B. Tilbrook. 2013. A climatology-based quality control procedure for profiling float oxygen data. J. Geophys. Res.: Oceans **118**: 5640–5650. doi:10.1002/jgrc.20399

Takeshita, Y., T. R. Martz, K. S. Johnson, and A. G. Dickson. 2014. Characterization of an ion sensitive field effect transistor and chloride ion selective electrodes for pH

measurements in seawater. Anal. Chem. **86**: 11189–11195. doi:10.1021/ac502631z

Takeshita, Y., T. R. Martz, L. J. Coletti, A. G. Dickson, H. W. Jannasch, and K. S. Johnson. 2017. The effects of pressure on pH of Tris buffer in synthetic seawater. Mar. Chem. **188**: 1–5. doi:10.1016/J.MARCHEM.2016.11.002

Takeshita, Y., T. Cyronak, T. R. Martz, T. Kindeberg, and A. J. Andersson. 2018. Coral reef carbonate chemistry variability at different functional scales. Front. Mar. Sci. **5**: 175. doi:10.3389/FMARS.2018.00175

Takeshita, Y., and others. 2021*a*. Accurate pH and O_2 measurements from spray underwater gliders. J. Atmos. Ocean. Technol. **38**: 181–195. doi:10.1175/JTECH-D-20-0095.1

Takeshita, Y., and others. 2021*b*. Consistency and stability of purified meta-cresol purple for spectrophotometric pH measurements in seawater. Mar. Chem. **236**: 104018. doi:10.1016/J.MARCHEM.2021.104018

Tengberg, A., and others. 2006. Evaluation of a lifetime-based optode to measure oxygen in aquatic systems. Limnol. Oceanogr.: Methods **4**: 7–17. doi:10.4319/lom.2006.4.7

U.S. Integrated Ocean Observing System (US IOOS). 2021. Manual for real-time quality control of water level data Version 2.1: A guide to quality control and quality assurance of water level observations. doi:10.25923/vpsx-dc82

Yin, T., and others. 2021. A novel lab-on-chip spectrophotometric pH sensor for autonomous in situ seawater measurements to 6000 m depth on stationary and moving observing platforms. Environ. Sci. Technol. **55**: 14968–14978. doi:10.1021/acs.est.1c03517

Acknowledgments

This work was funded by NSF OCE2300399, NSF OCE2300400, and the David and Lucile Packard Foundation. Dariia Atamanchuk, Mathieu Dever, Clark Richards and the rest of the Dalhousie Aquatron Flume team were instrumental in conducting the response time experiments. The Station M deployment and data collection was made possible by Ken Smith Jr., Alana Sherman, Rich Henthorn, and Paul McGill. Melissa Carter and Kayla Martin facilitated the deployment and recovery at Scripps Pier. We thank Jacki Long, James McClure, Chris Wahl, and Brent Jones for Spray glider preparation, deployment, and recovery.

Conflict of Interest

Christoph Staudinger was employed by PyroScience GmbH. All other authors declare no conflict of interest.

Submitted 17 June 2024
Revised 12 August 2024
Accepted 22 August 2024

Associate editor: Isaac Santos